INFECTION AND IMMUNITY, July 2006, p. 3790–3803 Vol. 74, No. 7
0019-9567/06/$08.00+0 doi:10.1128/IAI.00064-06

Early Events in *Mycobacterium tuberculosis* Infection in Cynomolgus Macaques†

Philana Ling Lin,[1] Santosh Pawar,[2] Amy Myers,[2] Amarenda Pegu,[3] Carl Fuhrman,[4] Todd A. Reinhart,[3] Saverio V. Capuano,[2,5]‡ Edwin Klein,[6] and JoAnne L. Flynn[2]*

Department of Pediatrics, Children's Hospital of Pittsburgh,[1] Department of Molecular Genetics and Biochemistry, University of Pittsburgh School of Medicine,[2] Department of Infectious Diseases and Microbiology, Graduate School of Public Health,[3] Department of Radiology, University of Pittsburgh Medical Center,[4] and Obstetrics, Gynecology, and Reproductive Sciences[5] and Division of Laboratory Animal Resources,[6] University of Pittsburgh School of Medicine, Pittsburgh, Pennsylvania 15261

Received 12 January 2006/Returned for modification 10 February 2006/Accepted 29 March 2006

Little is known regarding the early events of infection of humans with *Mycobacterium tuberculosis*. The cynomolgus macaque is a useful model of tuberculosis, with strong similarities to human tuberculosis. In this study, eight cynomolgus macaques were infected bronchoscopically with low-dose *M. tuberculosis*; clinical, immunologic, microbiologic, and pathologic events were assessed 3 to 6 weeks postinfection. Gross pathological abnormalities were observed as early as 3 weeks, including Ghon complex formation by 5 weeks postinfection. Caseous granulomas were observed in the lung as early as 4 weeks postinfection. Only caseous granulomas were observed in the lungs at these early time points, reflecting a rigorous initial response. T-cell activation (CD29 and CD69) and chemokine receptor (CXCR3 and CCR5) expression appeared localized to different anatomic sites. Activation markers were increased on cells from airways and only at modest levels on cells in peripheral blood. The priming of mycobacterium-specific T cells, characterized by the production of gamma interferon occurred slowly, with responses seen only after 4 weeks of infection. These responses were observed from T lymphocytes in blood, airways, and hilar lymph node, with responses predominantly localized to the site of infection. From these studies, we conclude that immune responses to *M. tuberculosis* are relatively slow in the local and peripheral compartments and that necrosis occurs surprisingly quickly during granuloma formation.

Mycobacterium tuberculosis remains a global health issue accounting for significant morbidity and mortality worldwide. In 2003, an estimated 2 million deaths occurred from tuberculosis (TB). Currently, one-third of the world's population is infected with *M. tuberculosis*, the causative pathogen in tuberculosis (27). Among those initially infected, a small percentage (5 to 10%) fail to control the initial infection and develop primary TB disease. The majority of humans infected with this organism mount an effective immune response that results in latent infection. However, reactivation of latent infection can occur years to decades later in a small subset of infected persons, leading to active TB. Early immunologic and pathological events during the course of infection as well as other factors may influence the outcome of *M. tuberculosis* infection. Understanding these early host-pathogen interactions is critical to our understanding of TB as well as for the development of vaccines, drug treatments, and diagnostic methods to eradicate this disease.

Although mice have been a valuable source of information regarding the initial and chronic immune responses to *M. tuberculosis*, certain features of human TB are not faithfully replicated in the mouse model. Murine granulomas are quite distinct in structure from human tuberculous granulomas. *M. tuberculosis*-infected murine lungs contain collections of T cells and macrophages, with tight clusters of B cells (24). However, necrosis of murine granulomas is almost always related to extremely high bacterial numbers, unlike human granulomas that commonly contain necrotic material. Human tuberculous granulomas have a more organized structure and can have several morphologically distinct forms, including solid (composed of organized lymphocytes and macrophages without necrosis), caseous (caseous necrosis in center of granuloma surrounded by lymphocytes and macrophages) with or without fibrosis, and calcified (mineralized) granulomas. Cavitary lesions within the lung (not seen in murine granulomas) are associated with high bacterial transmission, as they are presumed to represent erosion of an airway with direct communication to a necrotic granuloma. Moreover, different types of these granulomas can be observed in the same host. Despite these differences in granuloma structure, the murine granulomas serve to physically and immunologically contain the organisms and prevent dissemination and, thus, are similar in function to human granulomas. Granulomas in the rabbit, and even in the guinea pig, appear very similar to human granulomas; however, the paucity of available immunologic reagents for these models limit their use in defining the immunologic events during acute infection (reviewed in reference 6).

The nonhuman primate model of TB mimics all the pathological features of human TB and has the advantage of a large array of available immunologic reagents (3, 8, 10, 11, 26). Granulomas of the macaque model exhibit characteristics very

* Corresponding author. Mailing address: Department of Molecular Genetics and Biochemistry, University of Pittsburgh School of Medicine, W1157 Biomedical Science Tower, 200 Lothrop Street, Pittsburgh, PA 15261. Phone: (412) 624-7743. Fax: (412) 383-7220. E-mail: joanne@pitt.edu.

† Supplemental material for this article may be found at http://iai.asm.org/.

‡ Present address: Wisconsin National Primate Research Center, Madison, WI 53715.

TABLE 1. Descriptors and bacterial burden among nonhuman primates (*M. fasicularis*) after acute *M. tuberculosis* infection[a]

Monkey no.	Time p.i. (wk)	Necropsy score	CFU/ml in BAL fluid or result	Culture (GA) result	CFU/g of tissue in:	
					Hilar lymph node	Lung
12202	3	4	600	Negative	4×10^5	0
24002	3	2	Negative	Negative	2×10^{4}**	0
12302	4	1	Negative	Negative	4×10^3–5×10^3	0
24702	4	3	Negative	Negative	8.5×10^5	2×10^4–6×10^4
21902	5	10	Negative	Negative	4×10^4	2×10^{5}*
24102	5	9	Negative	Negative	1×10^{6}* 2.8×10^{6}*	3×10^4
22102	6	3	3	Positive	$3 \times 10^{4–6}$*	5.5×10^4
24302	6	8	Negative	Negative	8.3×10^{5}* 2×10^{5}**	2×10^4 1.1×10^{6}*

[a] Analyses were carried out at 3, 4, 5, and 6 weeks postinfection (p.i.). Necropsy scores were based on a formal pathologic assessment system (see supplemental material). High scores are associated with a greater degree of involvement (e.g,. >30 for advanced disease), whereas low scores reflect limited disease. Bacterial burden is measured in CFU either per volume or per gram in BAL fluid and tissue, respectively; culture is either positive or negative from gastric aspirate (GA) samples but not quantitated. *, bacterial burden from granulomatous tissue; **, bacterial burden from axillary lymph nodes. Greater bacterial burden is seen among granulomatous tissues, reflecting the localized nature of *M. tuberculosis* infection.

similar to human tuberculous granulomas that include cavitation, calcification, caseous necrosis, and multinucleated giant cells within affected lung and lymph nodes. In addition, following low-dose infection into the lungs, cynomolgus macaques can present with primary TB (40% of infected monkeys) or latent infection (60%) (3; also unpublished data). This is the only available model of true latent *M. tuberculosis* infection and, therefore, provides an opportunity to study aspects of this infection that cannot be approached in humans or other animal models.

The course of events leading to granuloma formation in humans is poorly understood. The sluggish induction of T-cell responses in the lymph nodes and subsequent migration of T cells to the lungs in the mouse model suggests that granuloma formation is slow. Studies of the guinea pig and rabbit models of infection suggest that primary granuloma formation occurs within the first 21 days after aerosol infection (reviewed in reference 14). The initial granuloma composition is not known, and early immunologic events are nearly impossible to study in human lungs. Most of what is known of human granulomas comes from autopsy studies or resected lungs from patients who have failed medical therapy. Thus, inferences regarding the "normal" pathological and immunologic progression of infection are biased. In this study, we describe the early responses of cynomolgus macaques during *M. tuberculosis* infection, focusing on the induction of immune responses in the blood, lymph nodes, lungs, and airway and granuloma formation. We found caseous granulomas as early as 4 weeks postinfection in the lungs and never found nonnecrotic granulomas in the lungs in these monkeys, in contrast to monkeys with active disease. Localized T-cell responses could be detected in the hilar lymph nodes and bronchoalveolar lavage (BAL) fluid by 4 weeks, and they increased throughout the course of infection. Phenotypic expression of T cells occurred in a compartmentalized fashion. These studies define early events in the course of *M. tuberculosis* infection in the primate model.

MATERIALS AND METHODS

Experimental animals. Eight adult male cynomolgus macaques (*Macacca fasicularis*) at least 4 years of age and between 4 to 10 kg in weight were used (Table 1). Animals were supplied by Buckshire Corporation (Perkasie, PA) or Labs of Virginia (Yemassee, SC) prior to infection. All monkeys were simian retrovirus type D negative. To assess the possibility of prior infection with *M. tuberculosis* and other confounding infectious agents, all monkeys were subjected to thorough health assessments, including a series of serologic and microbiologic tests (physical examination, complete blood count with differential, serum chemistry panel, erythrocyte sedimentation rate, direct fecal exam, stool culture, thoracic radiograph, tuberculin skin tests) while in quarantine. Baseline chest radiographs and tuberculin skin tests (TST) were normal and negative, respectively. Each animal was housed in a 4.3-ft^2 stainless steel cage and maintained in a biosafety level 3 suite. All animal protocols and procedures were approved by the University of Pittsburgh School of Medicine Institutional Animal Care and Use Committee.

Chemicals and reagents. Unless otherwise noted, all chemicals were obtained from Sigma Chemical Co. (St. Louis, MO). 7H10 agar was purchased from Difco Laboratories (Detroit, MI) and prepared according to the manufacturer's instructions. Antibodies for flow cytometric analysis were obtained from BD Pharmingen (San Diego, CA), BD Biosciences (San Jose, CA), or R & D Systems, Inc. (Minneapolis, MN).

Infection procedures. *M. tuberculosis* (Erdman strain; originally obtained from Trudeau Institute, Saranac Lake, NY) was passed through mice and frozen at −80°C in aliquots. An aliquot was thawed and diluted serially with phosphate-buffered saline (PBS) to the desired dose immediately before infection. Animals were then infected via bronchoscopic instillation of ~25 CFU/monkey in 2 ml of sterile 1× PBS to the right caudal or middle lung lobe, as previously described (3). An aliquot of the dilution was plated onto 7H10 agar plates and incubated at 37°C at 5% CO_2, and colonies were enumerated at day 21 to confirm the dose of bacterial inoculum.

BAL. BAL procedures have been previously described (3). In brief, animals were sedated and placed in a dorsal recumbent position. A 2.5-mm-outer-diameter flexible bronchoscope (Wolf Medical Instruments Incorporated, Vernon Hills, IL) was placed in the trachea and wedged into the right middle or lower lobe segment. A total of 40 ml of sterile saline was instilled briefly and suctioned for collection. Recovery of fluid was generally 75%. BAL fluid was then plated for bacterial burden determination, and cells were collected for immunologic assays (see below).

TST procedures. To confirm *M. tuberculosis* infection, TST and lymphocyte proliferation assays (LPA) were performed as previously described (3). Briefly, animals were sedated, and intradermal mammalian tuberculin (MOT; Synbiotics, Inc., San Diego, CA) was injected within the palpebra of the eyelid, as is the standard for primate skin testing. The eyelid was evaluated at 24, 48, and 72 h using a standardized grading system (19). A score of 3 or greater was considered positive. Two monkeys were not tested by TST (24002 and 24702); 24002 was necropsied at 3 weeks and 24702 had a positive LPA by 2 weeks postinfection.

Blood collection and radiographic procedures. As described previously (3), animals were sedated and blood samples collected by percutaneous femoral venipuncture using a Vacutainer system. Blood was obtained for immunologic assays and labs as described below. Radiographs were performed prior to infection and at biweekly intervals after infection. Animals were sedated while ventral-dorsal and right lateral thoracic radiographs were obtained. All radiographs were read by a board-certified pulmonary radiologist (C. Fuhrman).

Bacterial burden measurements. Serial dilutions of BAL fluid were plated onto 7H10 agar plates and incubated at 37°C with 5% CO_2. 7H10 plates were read 21 days later. Gastric aspirates were performed every 2 weeks using standard procedures described previously (3). Gastric aspirate fluid was assessed for *M. tuberculosis* by culture in a microbiology clinical laboratory (University of Pittsburgh Medical Center, Pittsburgh, PA).

ESR. Serial erythrocyte sedimentation rates (ESRs) were measured (in millimeters) using whole blood as described previously (3). This was performed before infection, biweekly postinfection, and at the time of necropsy. All samples were assayed in duplicate.

Necropsy procedures. Monkeys were randomly chosen to be euthanized at the predetermined time points of 3, 4, 5, and 6 weeks after infection. Two monkeys were used per time point. Immediately prior to necropsy, monkeys were sedated and a complete physical exam was performed. Animals were maximally bled using the Vacutainer system and euthanized with sodium pentobarbital (Schering-Plough Animal Health Corp, Union, NJ). All necropsies were conducted by a veterinary pathologist (E. Klein) as described previously (3). All tissues were obtained in a sterile fashion for immunology and microbiologic assays. Briefly, axillary and inguinal lymph nodes were obtained initially. The chest cavity was opened, and a gross examination of the organs was performed. The trachea, heart, and lungs were then removed en bloc. Gross pathological findings were notated during dissection of lung lobes and regional lymph nodes. Multiple cross sections of the lungs and lymph nodes were then performed to identify further gross histopathologic tuberculous lesions. The liver and spleen were also examined for evidence of disseminated infection, and samples were obtained for bacterial burden and histology. Based on the gross pathological findings, a numeric score was given to each monkey reflecting the degree of disease observed. A detailed gross pathological scoring system was used to assess the extent of disease in each monkey at necropsy, based on findings suspicious for TB with particular emphasis on lung-associated lymph nodes and lung lobes (see the supplemental material for the gross pathology scoring system). In general, the necropsy score was directly proportional to the degree of disease found at the time of necropsy. Representative sections of normal and abnormal appearing lung and lymph node were collected for histology, bacterial burden, RNA, and cell suspension for immunologic assays.

Histology. Tissue samples for histologic examination were placed in 10% normal buffered formalin and paraffin embedded. Sections (6 μm) were cut and stained with hematoxylin and eosin. Histology was reviewed by a veterinary pathologist (E. Klein). Criteria were established for all granulomas observed to objectively compare characteristics of granulomas between and within monkey groups by focusing on the size, type of granuloma (caseous, solid, suppurative, or mixed), distribution pattern (focal, multifocal, coalescing, and invasive), and cellular composition (absence or presence with degree of lymphocytic cuff, mineralization, fibrosis, multinucleated giant cells, and epithelioid macrophages).

In situ hybridization. Riboprobe synthesis and in situ hybridization (ISH) for CXCL9/Mig, gamma interferon (IFN-γ), tumor necrosis factor alpha (TNF-α), and *M. tuberculosis* 16S rRNA RNA targets were performed on tissue sections as previously described (4, 5, 7, 17).

Immunologic assays. Peripheral blood mononuclear cells (PBMCs) were obtained by standard Percoll (Amersham Bioscience, Piscataway, NJ) gradient purification and washed with sterile PBS. For tissues obtained at the time of necropsy, a cell suspension was produced using a MediMixer (BD Bioscience, San Jose, CA) homogenizer. PBMCs and cells from tissues were then divided for various assays.

Flow cytometric analysis. Immunophenotypic surface staining by flow cytometry (fluorescence-activated cell sorting [FACS]) was performed on PBMC, BAL fluid cells, and tissue cell suspensions from grossly appearing normal lung tissue, granulomatous lung tissue (when available), and regional lymph nodes. Cells were stained for CD3 (clone SP34; BD Pharmingen), CD4 (clone SK3; BD Bioscience), CD8 (clone SK1; BD Bioscience), CD11b (clone ICRF44; BD Bioscience), CD14 (clone MφP9; BD), CD29 (clone HUTS21; BD Pharmingen), CD69 (clone FN50; BD Pharmingen), CD45 (clone TU116; BD Pharmingen), CXCR3 (clone 1C6; BD Pharmingen), and CCR5 (clone 150503; R& D Systems). Cells were stained in at 4°C for 30 min. Cells were washed in FACS buffer (1× PBS, 2% human AB serum [Gemini Bioproducts, Calabasas, CA], 2% goat serum, 5% fetal bovine serum [Gibco, Invitrogen, Carlsbad, CA]) and fixed in 1% paraformaldehyde. Flow cytometric analysis was performed using CellQuest Software (BD Immunocytometry systems, San Jose, CA) and analyzed with Flow Jo software (Treestar, Inc, Ashland, OR).

DC isolation. Five to 7 days prior to the planned necropsy, PBMCs were incubated with 1× dendritic cell (DC) media (Iscove's modified Dulbecco's medium, 10% fetal bovine serum, 1,000 U/ml human granulocyte-macrophage colony-stimulating factor, 1,000 U/ml human interleukin-4) at a concentration of 8×10^6 PBMC/ml in a six-well plate (Corning Corp., Corning, NY) at 37°C with 5% CO_2. At day 3 to 5, 50% of the original volume was removed and replaced with fresh 2× DC media. The DCs were used as antigen-presenting cells for enzyme-linked immunospot (ELISPOT) on days 5 to 7.

ELISPOT assay. At least 1 day prior to use, 96-well multiscreen-immunoprecipitation filtration plates (Millipore Corp., Bedford, MA) were hydrated with serial washes of 70% ethanol, sterile deionized water, and 1× PBS and coated with anti-human/monkey IFN-γ antibody (15 μg/ml) (Mabtech, Nacka Strand, Sweden). Plates were kept at 4°C until the day of the ELISPOT assay, at which time the plates were washed with 1× PBS and blocked with RPMI and 10% human AB serum for 1 h at 37°C.

Each stimulator condition (including positive and negative controls) was performed in duplicate. Medium was used as a negative control. Positive controls consisted of a combination of phorbol 12,13-dubutyrate (12.5 μg/ml) and ionomycin (37.5 μg/ml) and another with mouse monoclonal anti-monkey CD3 antibody (30 μg/ml) (Biosource International, Camarillo, CA). The following mycobacterial protein stimulators were used at a concentration of 2 μg/ml unless otherwise noted: culture filtrate protein (CFP) (10 μg/ml), ESAT-6 (Rv3875) (10 μg/ml), 72F (Rv0125 and Rv1196), 38-1(CFP-10) (Rv3874), HTCC-1 (Rv3616c), 85a, TbH9 (Rv1196 and Rv1361c), MTI (Rv1793, Rv3619c, Rv1198, Rv1037c, and Rv2346c), DPAS (Mtb12), DPV (Rv1174c), MTCC-2 (Rv0915c), and Erd-14 (Rv2031c). Pools of peptides from the antigens ESAT-6 (Rv3875) and 38.1 (Rv3874) were also used (10 μg/ml) to enhance detection of CD8 T-cell responses. CFP and ESAT-6 proteins were obtained from the Tuberculosis Vaccine Testing and Research Materials Contract (NIH NIAID NO1-AI-40091, Colorado State University, Fort Collins, CO). All other proteins and peptides were generously donated from Corixa Corp., Seattle, WA.

PBMC ELISPOT assay was performed at 0, 2, 4, and 6 weeks postinfection as well as at the time of necropsy. PBMCs were added at a concentration of 2×10^5/well in RPMI and 10% human AB serum with each stimulator. At necropsy, ELISPOT assay was also performed on BAL fluid and tissue cells at a concentration of 1×10^5cells/well. With the exception of the PBMCs, DCs at a concentration of 5×10^3 DC/well were added. Additional control wells included DCs alone (without specific stimulator) with the cells of interest and *M. tuberculosis*-infected DCs. For the latter controls, DCs were infected at a multiplicity of infection of 4 over 4 h the morning of the necropsy. Cells were incubated for ~40 h at 37°C with 5% CO2.

ELISPOTs were developed by lysing the cells with 200 μl of deionized water to each well for 10 min. The plates were then washed with 0.05% Tween 20 in 1× PBS. Biotinylated anti-human IFN-γ antibody (Mabtech, Nacka Strand, Sweden) (2.5 μg/ml) was added to each well and allowed to incubated at 37°C with 5% CO_2 for 2 h. After multiple washes with 0.05% Tween 20 in 1× PBS, streptavidin-horseradish peroxidase-Q (Mabtech) was then diluted 1:100, added to each well, and placed at 37°C for 1 h. Spots were stained using the AEC peroxidase kit per the manufacturer's recommendations (Vector Laboratories, Inc., Burlingame, CA). The number of spots was determined with an automatic ELISPOT reader.

Statistical analysis. As we could not prove that our data fit a normal distribution, pairwise comparison of cellular numbers by FACS was analyzed using Wilcoxon test, with a P value of <0.05 considered significant.

RESULTS

Clinical and immunologic response to *M. tuberculosis*-infected monkeys. All eight monkeys were clinically well during the course of infection. There were no overt clinical signs consistent with active TB disease, including cough, weight loss, decreased appetite, or other behavioral changes. In one monkey (24702), a right lower lobe infiltrate was observed on postinfection day 10 and later resolved. The other monkeys had normal chest radiographs throughout the time of infection and at necropsy. Our previous results suggest that increased ESR, a nonspecific measure of inflammation, correlates with active tuberculosis (3, 23, 26). Erythrocyte sedimentation rates remained low (<2 mm) during the course of infection.

Conversion from a negative to positive TST was observed by 5 weeks postinfection. To further establish that monkeys were infected, proliferation to purified protein derivative or CFP by LPA was seen in 6 of 8 monkeys; the two monkeys that did not

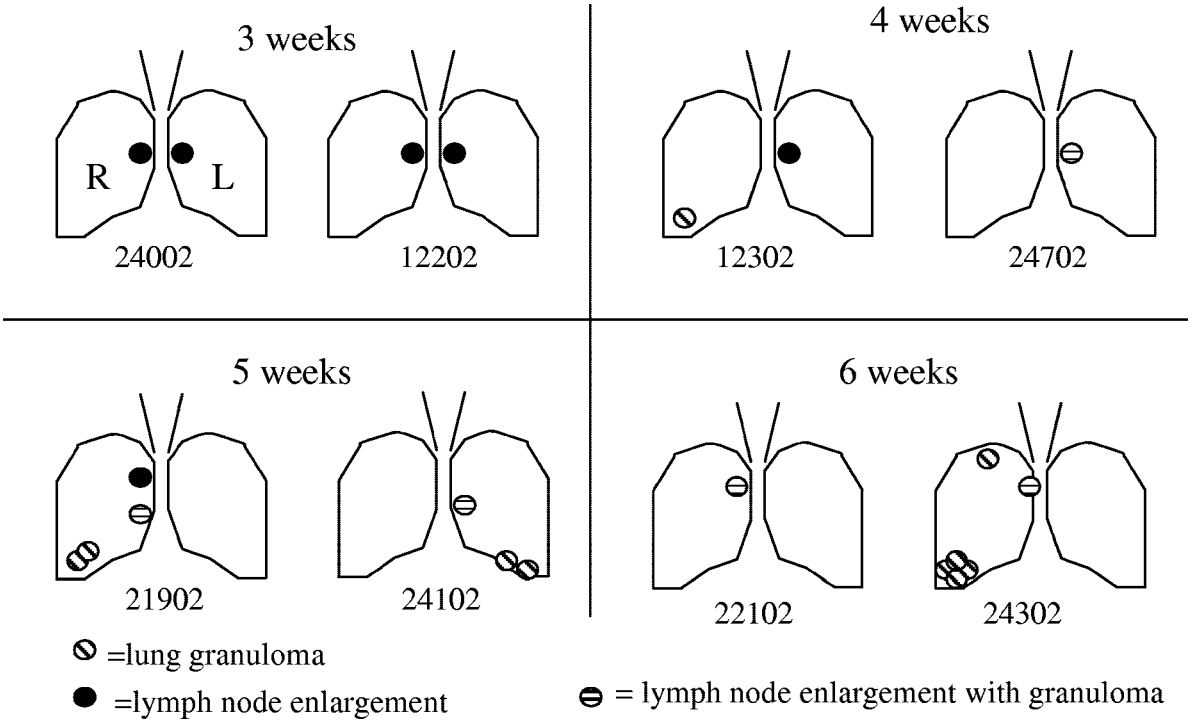

FIG. 1. *M. tuberculosis* infection progresses from lymph node to lung granuloma by gross and microscopic histopathology 3, 4, 5, and 6 weeks postinfection in nonhuman primates. Hilar lymph node enlargement and granuloma formation was observed at 3 and 4 weeks postinfection, respectively. Granuloma formation is seen in the lower lung lobes by 5 weeks postinfection. R, right; L, left.

respond were euthanized at 3 and 4 weeks. It is likely that one or both would have converted to positive by LPA at a later time point, as demonstrated by our prior studies (3; also unpublished data).

Gross and microscopic histopathology at necropsy. We observed a progression of granuloma formation from the lymph nodes to the lungs over time (Fig. 1). Monkeys euthanized at 3 weeks had bilaterally enlarged hilar lymph nodes without gross evidence of granuloma formation in the lungs. No evidence of microscopic granuloma formation was observed in the lymph node or lungs at 3 weeks postinfection. By 4 weeks postinfection, both monkeys also had enlarged hilar lymph nodes. Monkey 24702 had one small (<2 mm) focal granuloma in the left hilar lymph node. Both early and more advanced granuloma formation was seen within draining thoracic lymph nodes of this same monkey. Multiple solid, unorganized aggregates of epithelioid macrophages with infrequent multinucleated giant cells were observed within the hilar nodes of the same monkey (Fig. 2A), indicating lymphatic spread of the infection. More advanced nodal lesions were observed in the contralateral hilar lymph node of the same monkey characterized by early, poorly organized, multifocal, and coalescing areas of granulomatous inflammation with mild central necrosis. Despite the lack of obvious lesions in the lung by gross assessment, by 4 weeks postinfection, areas of caseous granuloma formation were observed in the right lower lobe of monkey 12302 by microscopic evaluation (Fig. 2B). In monkeys with active TB from other studies, we generally observe both caseous and solid (cellular) granulomas, as depicted in Fig. 2E and F for comparison.

A greater degree of pathology was observed by 5 to 6 weeks postinfection. One monkey at 5 weeks and one at 6 weeks postinfection had enlarged hilar lymph nodes with evidence of coalescing caseous granulomas by gross examination. By 5 weeks postinfection, classic granuloma formation was observed in the cranial hilar lymph nodes of monkey 21902 (Fig. 2C). These lesions were comprised of large areas of central caseation surrounded by a dense mantel of epithelioid macrophages. A band of coagulative change was observed immediately within the outer margin of caseation. In addition, "satellite" foci comprised of poorly circumscribed areas of early stage granulomatous inflammation were seen adjacent to larger primary lesions, suggesting contiguous spread via direct extension. Multifocal and coalescing caseous granulomas were observed in the right lower lung of monkey 21902 at 5 weeks postinfection (Fig. 2D). At 6 weeks postinfection, complete effacement of lymph node structure by granuloma formation was present. Organized granulomas were seen in the hilar lymph nodes at 6 weeks postinfection consisting of large regions of central caseation and prominent palisading of epithelioid macrophages in the surrounding zone. However, several visible caseous granulomas (varying in size from 1 to 4 mm) were observed in the lower lung lobes of the other monkeys necropsied at 5 and 6 weeks postinfection. A large granuloma formed by multiple smaller coalescing foci was present in the right lower lobe of the lung of monkey 24302 as well. With the exception of occasional solid, unorganized aggregates of macrophages that may represent early granuloma development in the lymph nodes at 4 weeks postinfection, all granulomas examined microscopically were caseous in nature. These data indicate that even low-dose *M. tuberculosis* infection causes

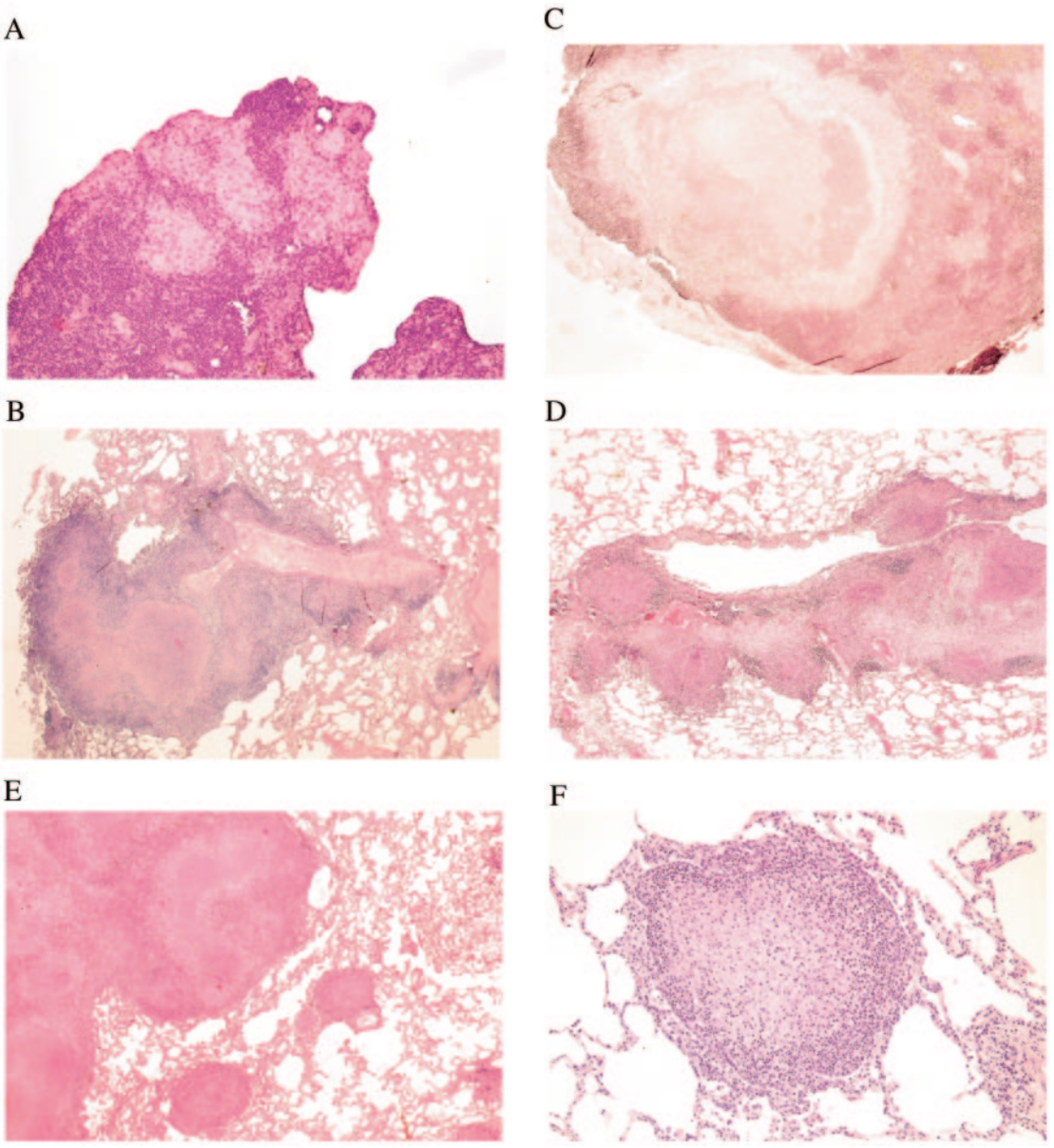

FIG. 2. Microscopic pathology of granuloma formation in acute *M. tuberculosis* infection of nonhuman primates in which progression from early unorganized granulomas was observed only in the lymph node. All granulomas identified in the lungs were caseous granulomas. (A) Unorganized aggregates of epithelioid macrophages representing early granuloma formation were observed in the left hilar lymph nodes of a monkey (24702) at 4 weeks postinfection. Magnification, ×10. (B) Caseous granuloma formation observed in the right lower lobe of a monkey (12302) at 4 weeks postinfection. Magnification, ×2. (C) Well-organized caseous granulomas were observed in the hilar lymph nodes of a monkey (21902) by 5 weeks postinfection. Magnification, ×2. (D) Multifocal, coalescing, classic appearing caseous granulomas observed in the right upper lobe of a monkey (21902) at 5 weeks postinfection. Magnification, ×2. (E) Both solid (lower two granulomas) and caseous (upper portion) granulomas are seen within the same monkey lung. Coalescing caseous granulomas in which eosinophilic proteinaceous material are seen centrally with peripherally located epithelioid macrophages and lymphocytes. Magnification, ×2. (F). Higher magnification of the same section seen in panel E demonstrating a classic solid granuloma that is composed predominantly of epithelioid macrophages centrally surrounded by lymphocytes peripherally. Other inflammatory cell types are dispersed throughout the granuloma. No necrosis or caseation is seen (hematoxylin and eosin staining). Magnification, ×10.

discernible pathological changes within a relatively short period of time.

Microbiologic analysis of BAL and gastric aspirate fluid of infected monkeys. In human infection, *M. tuberculosis* can be recovered from sputum, gastric aspirate fluid, and/or BAL fluid, and therefore, these fluids can be used for diagnostic purposes. While it is not possible to obtain sputum from monkeys, gastric aspirate and BAL fluid can be obtained. Our previous studies indicated that *M. tuberculosis* growth from BAL fluid occurred in monkeys with active disease but rarely in monkeys considered to have latent infection (3). Based on our growing experience with this model, it is also not uncommon to detect *M. tuberculosis* in BAL fluid from monkeys within the first 2 months of infection (unpublished data). In the current

infections, BAL was only performed at necropsy, due to the limited duration of the study. BAL fluid from two monkeys was positive for *M. tuberculosis* (Table 1) but negative for all other monkeys. Thus, *M. tuberculosis* can be present in the airways shortly after infection, but this may be a transient phenomenon.

Gastric aspirate fluid was obtained from the monkeys on a biweekly basis after infection. In parallel with BAL fluid cultures, *M. tuberculosis* growth from gastric aspirate fluid is seen among monkeys with active disease and is occasionally positive during the first 2 months of infection (3). In these early infection studies, the gastric aspirate culture was positive from only one monkey (22102) 4 weeks after infection. This particular sample was positive by culture but was acid-fast smear negative, suggesting a low bacterial level. As noted above, this monkey also had *M. tuberculosis* growth in the BAL fluid at necropsy, although at a low level (Table 1).

Microbiologic analysis of tissues obtained at necropsy. At necropsy, samples from each lung lobe, lung-associated lymph nodes, any obvious granulomas, axillary and inguinal lymph nodes, spleen, and liver were processed to obtain cells for immunologic analysis and plated for enumeration of *M. tuberculosis* growth. Due to differences in sizes of tissue samples, bacterial numbers are reported as CFU per gram of tissue. It is possible to fail to detect bacteria due to sampling error, particularly in the lungs, as the lobes are relatively large and the disease tends to be localized, as indicated in the histologic analysis.

The bacterial burden appeared in localized areas of infection. With the exception of one monkey (24002), *M. tuberculosis* was detected in the hilar lymph nodes of all infected monkeys at necropsy (Table 1). Of note, monkey 24002 had *M. tuberculosis* growth in the axillary lymph node sample. Both of the monkeys infected for 3 weeks, and one of the monkeys infected for 4 weeks harbored 0.4×10^4 to 85×10^4 CFU/g of lymph node tissue. Monkeys at 5 and 6 weeks postinfection (as well as one monkey at 4 weeks postinfection) had higher bacterial numbers (0.04×10^6 to 3×10^6 CFU/g) in the lymph node. *M. tuberculosis* was not cultured from the lung tissue of either monkey at 3 weeks postinfection nor from one monkey at 4 weeks postinfection. *M. tuberculosis* was detected in both granulomatous and nongranulomatous lung tissue of the other monkey at 4 weeks and in all monkeys necropsied at 5 and 6 weeks. Among grossly apparent granulomas, bacterial numbers were between 0.2×10^6 to 3×10^6 CFU/g. In lung tissues without macroscopic granulomas, the bacterial burden was either undetectable or ranged from 2×10^4 to 5×10^4 CFU/g, indicating that most bacteria within the lungs were sequestered in the larger visible granulomas. One of the monkeys at 6 weeks postinfection (24302) had grossly visible granulomas in multiple lung lobes. This suggests that the initial infection can spread relatively quickly to multiple lobes. Granulomas observed in lobes distal to the site of infection (as is the case of a right upper lobe granuloma) and those seen on both sides of the lung are suggestive of hematogenous dissemination occurring early after infection. No bacteria were detected in the spleen or liver in any of these monkeys, but two monkeys (24002 and 24302) had culturable bacteria in axillary lymph nodes.

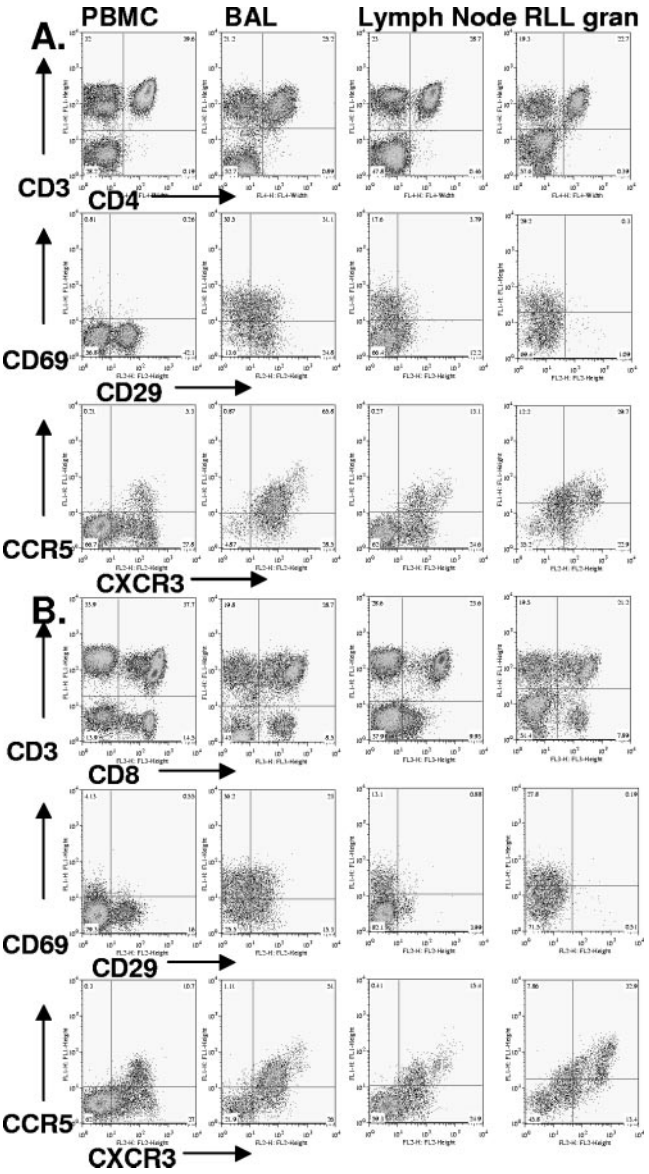

FIG. 3. Phenotypic characterization of T cells from various sites. Cells from PBMCs, BAL fluid, hilar lymph node, and right lower lobe granulomatous lung (RLL gran) were stained for CD3, CD4 (A), and CD8 (B) (top row). Cells were gated on $CD4^+$ (A) or $CD8^+$ (B) cells and analyzed for expression of activation markers CD69 and CD29 (middle rows of panels A and B) or for chemokine receptors CCR5 and CXCR3 (lower rows of panels A and B). Results for a representative monkey (24302) are shown. Compiled results for all monkeys are presented in Fig. 4.

Phenotypic characterization of PBMCs, BAL fluid, and tissue cells. Flow cytometry was performed to define the phenotypic characteristics of cells from blood, BAL fluid, and tissues at necropsy. The percentage of $CD4^+$ $CD3^+$ T cells (33% ± 7%) and $CD8^+$ $CD3^+$ T cells (35% ± 5%) in the PBMCs did not change over the course of infection and did not differ significantly from pooled data from uninfected monkeys ($CD4^+$ $CD3^+$, 37% ± 9%; $CD8^+$ $CD3^+$, 32% ± 14%). In cells recovered by BAL, the T-cell percentages were variable ($CD4^+$ $CD3^+$, 23% ± 8%; range, 17 to 42%; $CD8^+$ $CD3^+$,

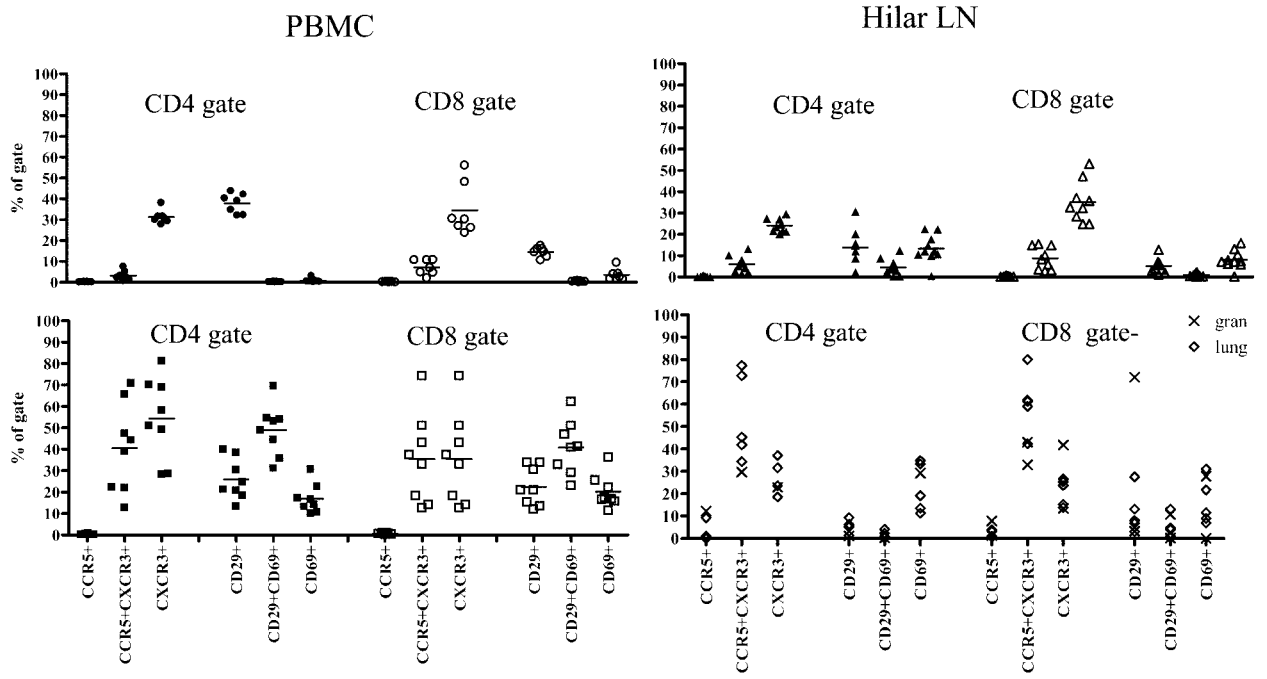

FIG. 4. Compartmentalization of the activation markers and chemokine receptors on CD4 and CD8 T cells among PBMCs, hilar lymph node (hilar LN) cells, BAL fluid cells, and lung cells (both granulomatous and nongranulomatous) of eight *M. tuberculosis*-infected cynomolgus macaques at 3 to 6 weeks postinfection. Cells from monkeys at all time points were analyzed by flow cytometry. Within the lymphocyte gate, cells were gated on CD4 or CD8 cells, then the percentage of single positive cells (CD29, CD69, CXCR3, or CCR5) or double positive cells ($CD29^+$ $CD69^+$ or $CXCR3^+$ $CCR5^+$) in the gate were reported. The median of each group is depicted. Patterns of activation markers and chemokine receptors differed in their pattern of expression depending on the location of CD4 and CD8 T cells. There were no differences in the activation marker expression over time. Due to the limited number of lymphocytes obtained in lung samples, lung sections here are from weeks 5 and 6 postinfection.

19% ± 10%; range, 7 to 39%). This profile was not significantly different from BAL fluid of uninfected animals (data not shown). There was no obvious trend towards increasing T-cell numbers or percentages over the 6 weeks of infection. In hilar lymph nodes, there were 36% ± 9% $CD4^+$ $CD3^+$ T cells and 24% ± 6% $CD8^+$ $CD3^+$ T cells, without an obvious change in percentages over the 6-week course of infection. Within the lung tissue of the monkeys, there were very few T cells detected at necropsy, and there was substantial variability, due to sampling. Due to scarcity of granuloma tissue and the need to perform multiple assays, phenotypic characterization of T cells was not performed on all tissue samples and granulomas from the lung. There were also several samples of granulomatous lung tissue obtained that did not have sufficient T cells to be analyzed completely. In the grossly normal lung tissue samples with sufficient T cells (~2 lung tissue samples per monkey) analyzed, 1.8% ± 3.5% of the live cells were $CD4^+$ $CD3^+$ T cells, and 2.1% ± 3.3% were $CD8^+$ $CD3^+$ T cells. However, in the monkeys euthanized at 6 weeks, the average percentages of CD4 and CD8 T cells increased ($CD4^+$ $CD3^+$, 4.1% ± 6.1%; $CD8^+$ $CD3^+$, 4.5% ± 5.3%), suggesting more T-cell infiltration into the lungs as the infection progressed (consistent with the histologic findings). However, there was still substantial variability among specimens, most likely due to the localized nature of *M. tuberculosis* infection. When an excised granuloma from the right lower lung lobe of a 6-week-infected monkey was analyzed, T-cell percentages were dramatically increased ($CD4^+$ $CD3^+$, 13.3%; $CD8^+$ $CD3^+$, 12.5%). This clearly indicates an enrichment of T cells at the local site of infection within the lungs. An example of phenotypic expression of markers on T cells from multiple sites examined by flow cytometry in a 6-week-infected monkey is depicted in Fig. 3.

Activation phenotype of cells from infected monkeys. The activation status of the T cells within each compartment was assessed using two markers: CD69, generally thought to be a marker of early T-cell activation, and CD29, another marker of T-cell activation, sometimes referred to as a late activation marker (16). There was a different distribution of these activation markers on the T cells from blood, BAL fluid, lymph nodes, and lung tissue. Cells were gated on either CD4 or CD8 and then analyzed for activation marker expression (Fig. 3 and 4). Activation phenotypes of PBMCs done at the time of necropsy for all time points demonstrated that 30% ± 10% of the CD4 T cells were positive for CD29, but <1% were positive for CD69. In the CD8 gate, 13% ± 3% were $CD29^+$, while 8% ± 3% were $CD69^+$. Only 1% were positive for both CD29 and CD69. There was no obvious change in the activation patterns over the 6 weeks of infection.

Activation patterns in the BAL T cells were different than in other compartments (Fig. 4). First, the majority (>85% for CD4, >80% for CD8) of T cells recovered from the alveolar spaces were activated, as indicated by expression of one or both of the activation markers, CD29 and CD69. Although there were high percentages of CD4 and CD8 T cells that were

positive for either CD29 or CD69, the most striking finding was the high percentage of cells that were positive for both activation markers (CD4, 49%; CD8, 41%). This pattern of activation markers was not obviously different from that of BAL cells from uninfected monkeys (data not shown).

In the hilar lymph nodes, ~34% of the CD4 T cells and only 14% of the CD8 T cells were activated in the infected monkeys at necropsy (Fig. 4), and this did not change appreciably depending on the length of infection, up to 6 weeks (hilar lymph nodes from uninfected monkeys were not examined). Although most of the activated cells were either $CD29^+$ or $CD69^+$, there was a small subset (4.5%) of $CD29^+$ $CD69^+$ cells in the CD4 population, although very few in the CD8 T-cell population. Those lymph nodes with grossly visible granulomas did not have substantially different patterns of activation marker expression compared to visibly normal lymph nodes from these monkeys.

Despite numerous lung samples obtained, there were only small numbers of T cells present in grossly normal specimens. Nonetheless, an activation pattern distinct from that of the other compartments was observed. Approximately 30% of the CD4 T cells and 33% of the CD8 T cells had at least one activation marker. However, the majority of these activated CD4 T cells were positive only for CD69, with very few that were $CD29^+$. In the CD8 T-cell population, cells either had CD69 only (12%) or CD29 only (17%). This distribution is quite distinct from that seen in the T cells recovered from the airways. T cells from the grossly visible granuloma analyzed from monkey 24302 (6 weeks postinfection) were not substantially different in the activation pattern compared to T cells isolated from lung samples of the other monkeys, except in the CD8 population, where there was a much lower percentage of $CD29^+$ (0.5%) or $CD69^+$ $CD29^+$ (0.2%) cells and a higher $CD69^+$ (28%) subset of cells isolated from the granuloma. Of course, there were many more T cells present in the granuloma-containing specimens than in lung tissue without grossly obvious granulomas.

Chemokine receptor expression on T cells from infected monkeys. Chemokines and chemokine receptors are known to play an important role in immune cell migration to the site of inflammation both to and within tissues. We and others have previously published studies showing that *M. tuberculosis* induces chemokine expression by murine and human macrophages (1, 18, 20, 21). We also demonstrated strong expression of CXCR3 ligands (CXCL9, CXCL10, and CXCL11) and the presence of CXCR3-expressing T cells within the granulomas of monkeys with active disease (7). To identify chemokine receptors expressed early in infection within various compartments of the host, we determined the expression of CXCR3 and CCR5 on T cells in the monkeys at necropsy (Fig. 3 and 4). In PBMCs, ~31% ± 3% of the CD4 T cells were $CXCR3^+$, and a small percentage (3% ± 2%) were positive for both CXCR3 and CCR5. In the CD8 T-cell population, 35% ± 12% were CXCR3 single positive, while 7% ± 4% were $CXCR3^+$ $CCR5^+$. CD4 or CD8 T cells positive for CCR5 alone were not detected in the PBMCs.

In contrast to PBMC, the vast majority (>90%) of T cells recovered from BAL fluid were positive for these chemokine receptors. Most of the CD4 and CD8 T cells were either $CXCR3^+$ or $CXCR3^+$ $CCR5^+$. There were no CCR5 single positive T cells in the BAL fluid. A similar pattern of chemokine receptor expression was observed in BAL cells from uninfected animals (data not shown). In the hilar lymph nodes, ~30% of the CD4 and ~44% of the CD8 T cells were positive for these chemokine receptors. Most of these were CXCR3 single positive, with a small percentage $CXCR3^+$ $CCR5^+$.

TABLE 2. Percentage of chemokine receptor-expressing T cells in the lungs[a]

No. of wks p.i.	% of cells expressing chemokine receptor within T-cell population					
	CD4			CD8		
	$CCR5^+$	$CXCR3^+$	$CCR5^+$ $CXCR3^+$	$CCR5^+$	$CXCR3^+$	$CCR5^+$ $CXCR3^+$
3–4	3 ± 3	39 ± 12	37 ± 8	3 ± 3	29 ± 9	43 ± 5
5–6	4 ± 5	25 ± 7	50 ± 20	3 ± 2	23 ± 10	54 ± 15

[a] Mean percentages and standard deviations of chemokine receptors within CD4 or CD8 lymphocyte gates are shown. While there was no statistical significance, there was a trend toward more double positive ($CXCR3^+$ $CCCR5^+$) cells at the later time points p.i.

In the lung, as mentioned previously, there were fewer T cells to analyze than in the other tissues sampled. However, the pattern was distinct from PBMCs, BAL fluid, and lymph nodes. Most (79%) of the T cells expressed one or both of these chemokine receptors, and the pattern was similar between CD4 and CD8 T cells, with the majority expressing both CXCR3 and CCR5. Most of the remaining cells expressed CXCR3 alone, but in contrast to the other tissues, there was a small percentage of CCR5 single positive cells. Although we did not detect obvious changes in the pattern of chemokine receptor expression over the 6 week-course of infection in PBMCs, BAL fluid, or lymph node cells, there was a trend towards more cells expressing both CXCR3 and CCR5 and fewer cells expressing CXCR3 alone in the lungs of monkeys euthanized at the later time points (5 and 6 weeks) compared to earlier time points (3 and 4 weeks) (Table 2). This suggests that the T cells in the lungs acquire the CCR5 marker as the infection progresses or that more cells bearing both CXCR3 and CCR5 migrate to the lungs of monkeys with more disease.

PBMC IFN-γ production during early *M. tuberculosis* infection. ELISPOT assays for IFN-γ were performed to monitor T-cell responsiveness over the course of infection in the PBMC. While a broad number of mycobacterial antigens were used in each ELISPOT assay (see Materials and Methods), we will focus on the mycobacterial antigens that showed responses during the course of infection (Fig. 5). Prior to infection, four (24702, 21902, 22102, and 24102) of the eight monkeys had positive responses to CFP, although not to the *M. tuberculosis*-specific protein ESAT-6 (Rv3875). Because CFP is a mixture of mycobacterial antigens, these results likely reflect cross-reactivity of nontuberculous mycobacterium infection among monkeys who were housed in outside environmental facilities. The response to CFP in these monkeys did not increase after infection. None of the eight monkeys had positive PBMC responses to the other mycobacterial antigens used in the ELISPOT assay prior to infection.

Five of the eight monkeys had IFN-γ production specific to CFP by ELISPOT as well as at least one other antigen by 2 weeks postinfection. The following three monkeys did not show in-

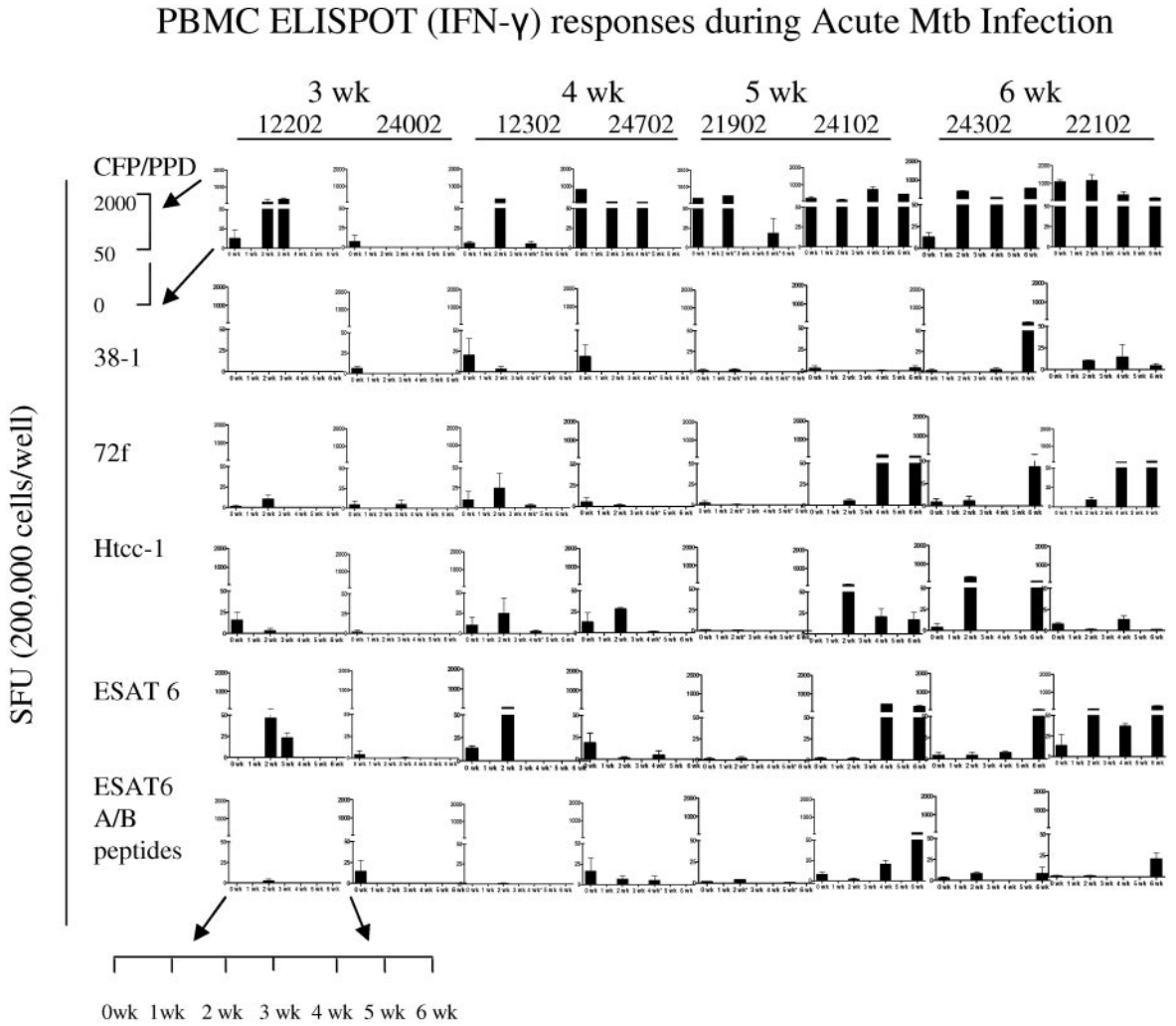

FIG. 5. Greater magnitude and broader responses to mycobacterial antigens are seen over time from serial PBMC IFN-γ responses to selected antigens (CFP, 38-1 [CFP-10, Rv3874], 72f [Rv0125 and Rv1196], HTCC-1 [Rv3616c], ESAT6 [Rv3875], and ESAT6 peptides) by ELISPOT assay during acute *M. tuberculosis* infection. Antigen responses were measured in spot-forming units (SFU) preinfection and every 2 weeks until the time of necropsy (3, 4, 5, and 6 weeks postinfection). *y*-axis increments are at 0, 25, 50, 1,000, and 2,000 SFU. Responses of at least 25 were considered positive. Five monkeys had positive responses to CFP preinfection, reflecting possible cross-reactivity to other environmental mycobacterial species. In general, responses to only CFP were observed at 3 and 4 weeks. A greater magnitude of responses to a broader spectrum of antigens was seen by 5 and 6 weeks after infection.

creases in responses to more than one antigen by ELISPOT postinfection: 24002 (necropsied at 3 weeks), 24702 (necropsied at 4 weeks), and 21902 (necropsied at 5 weeks). Responses to HTCC1 (Rv3616c) and ESAT-6 (Rv3875) were seen as early as 2 weeks postinfection. By 4 to 6 weeks postinfection, responses to 38-1 (Rv3874) and 72-F (Rv0125 and Rv1196) were observed. By 5 to 6 weeks postinfection, most monkeys had IFN-γ production to multiple antigens. Thus, as the infection progressed, IFN-γ responses of a higher magnitude (frequency of response) and to a broader range of mycobacterial antigens were observed. This has also been observed in our studies with monkeys with longer term infections, in which the immune response initially broadens in the periphery and then is reduced as the infection is controlled (data not shown). The three monkeys with marginal or no increased peripheral responses postinfection did not seem to differ substantially from the other monkeys in their necropsy groups with respect to bacterial numbers or pathology (though limited by sample size).

IFN-γ production by the BAL T cells of monkeys early in infection. Cells were obtained from BAL fluid at necropsy and stimulated with autologous, PBMC-derived DCs pulsed with various mycobacterial antigens, and the number of cells producing IFN-γ was determined by ELISPOT. Due to the limited numbers of cells obtained from BAL fluid, a smaller panel of antigens was used. The total number of BAL cells/ml obtained during acute infection was not substantially different at each time point. Only 2 of the 4 monkeys at 3 and 4 weeks postinfection had positive IFN-γ responses to CFP. IFN-γ production to other antigens was not observed at these early time points. By 5 to 6 weeks after infection, IFN-γ production to at least one other antigen in

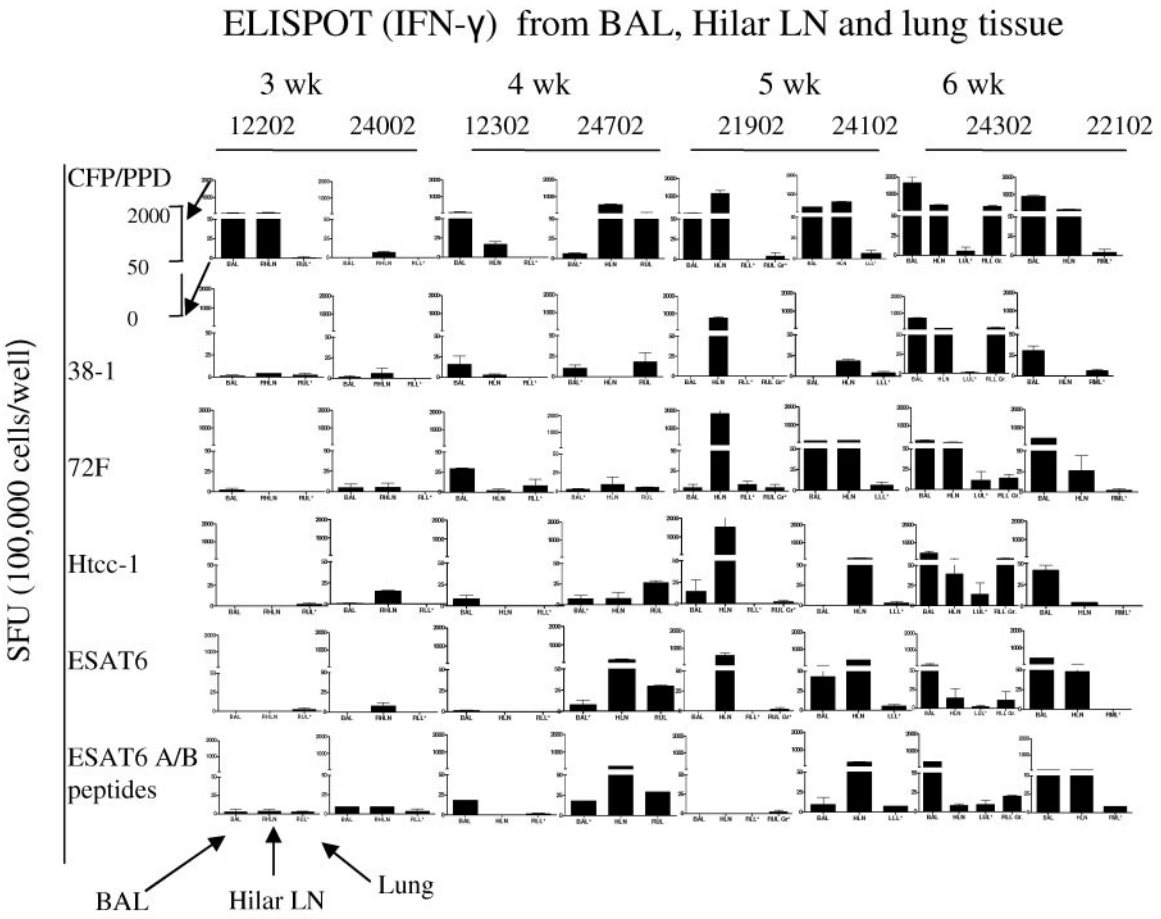

FIG. 6. Broader BAL fluid-, lymph node (LN)-, and lung (with or without granuloma)-specific IFN-γ responses to mycobacterial antigens (CFP, 38-1 [CFP-10, Rv3874], 72f [Rv0125 and Rv1196], HTCC-1 [Rv3616c], ESAT6 [Rv3875], and ESAT6 peptides) seen over time by ELISPOT assay at 3, 4, 5, and 6 weeks after *M. tuberculosis* infection. Antigen responses were measured in spot-forming units (SFU). *y*-axis increments are at 0, 25, 50, 1,000, and 2,000 SFU. Responses of at least 25 SFU were considered positive. IFN-γ responses to CFP occurred early in the course of infection. By 5 and 6 weeks after infection, IFN-γ responses were observed with a broader spectrum of antigens. Few responses were observed among lung tissue given the paucity of lymphocytes among tissue samples, with the exception of granulomatous lung tissue that was enriched with lymphocytes.

addition to CFP was observed from BAL cells of 3 of the 4 monkeys.

IFN-γ responses in tissues of infected monkeys. We focused on the immunologic responses of the lung and mediastinal lymph nodes for several reasons. Based on the gross pathological findings and our growing experience with monkeys with long-standing active disease, we anticipated that IFN-γ responses would likely be strongest in the lung and draining lymph nodes of the lung. This is supported by studies in the murine model in which mediastinal lymph nodes are the site of mycobacterium-specific T-cell priming and are a source of culturable *M. tuberculosis*. ELISPOT analysis of T-cell responses in the lymph nodes of monkeys euthanized at 3 to 4 weeks postinfection revealed responses to CFP or other antigens in 2 of the 4 monkeys. All 4 monkeys euthanized at 5 and 6 weeks postinfection had strong IFN-γ responses to CFP and at least 3 other antigens. Thus, recapitulating trends seen in PBMCs and BAL fluid, early after infection, IFN-γ production appeared primarily to CFP, but as the course of infection continued, responses to a broader spectrum of antigens was observed.

The paucity of T cells observed within the lung limited detection of IFN-γ production. Moreover, only a small number of T cells could be obtained from granulomatous lung tissue samples due to the size of the lesions, the presence of necrosis in the lesions, and the small number of lesions present per monkey. Thus, meaningful analysis of T-cell responses in the lungs was limited. This likely reflects the early stages of the infection, as we are able to recover more T cells from monkeys with active disease. In one monkey (24702) at 4 weeks postinfection, a positive response to CFP was observed. T cells from the right lower lobe of a monkey (24302) at 6 weeks postinfection had IFN-γ responses to CFP, 38-1 (Rv3874), and HTCC-1 (Rv3616c). Antigens that elicited a positive response in cells from the lung correlated with positive responses to that same antigen in BAL or hilar lymph node cells but not vice versa. Thus, as seen previously, T cells obtained from the granuloma in the lymph nodes or lung tissues of the monkeys at 5 to 6 weeks gave a stronger and broader

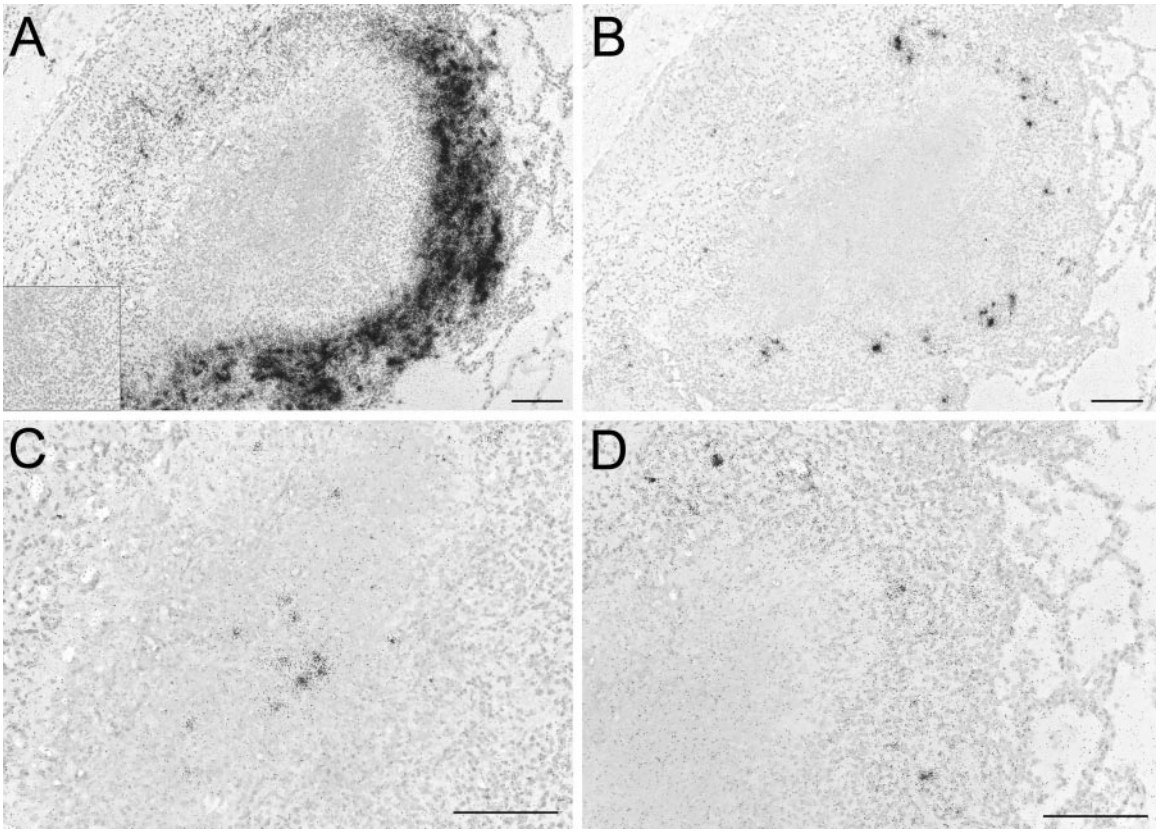

FIG. 7. In situ detection of cellular and *M. tuberculosis* RNAs in a pulmonary granuloma. In situ hybridization was performed on pulmonary tissues from animal 21902, using ^{35}S-UTP-labeled riboprobes specific for CXCL9/Mig (A), IFN-γ (B), mycobacterial 16S rRNA (C), and TNF (D) RNAs. The inset in panel A is a cropped image (same magnification) of ISH with a sense control riboprobe on a subjacent tissue section. Bar, 100 μm.

response to the various antigens. Similarly, this pattern was observed in the BAL fluid and PBMCs, although there were differences in the specific type of antigens recognized by the cells from BAL fluid or lung tissue (Fig. 6).

In situ distributions of host and mycobacterial RNAs. We used in situ hybridization to identify the localized expression of *M. tuberculosis* 16S rRNA, CXCL9 (a CXCR3-binding chemokine), IFN-γ, and TNF RNA targets in lung tissue specimens from these monkeys using multiple sections from each sample. In all of the tissues examined, CXCL9 mRNA was abundantly expressed only in lung tissues containing granulomatous lesions and only in association with the lesions. The intense CXCL9 in situ hybridization signal was localized in a thick band of cells surrounding the acellular centers of caseous granulomas. This pattern of CXCL9 expression was similar to that previously observed in animals infected with active disease and at more advanced stages of infection (7). We found that the mRNAs for TNF and IFN-γ were expressed at high levels and, in some cases, in appreciable numbers of cells, all of which were intimately associated with the granulomas and localized within the cellular shell comprising the outer regions of the granulomas (Fig. 7 and data not shown). Cells expressing these cytokine mRNAs were rarely localized away from the granulomas. Finally, to assess localization of *M. tuberculosis*, we performed in situ hybridization with a mycobacterial 16S-rRNA-specific riboprobe. In all the granulomas examined, the mycobacterial 16S rRNA ISH signal could be found only in the granulomatous regions of lung tissues and was localized specifically to the central, acellular regions of caseous granulomas. These findings indicate that pulmonary granulomas that develop during initial stages of infection are similar to those that are present in the active phase of disease with respect to the expression of these selected host response genes and the distribution of *M. tuberculosis* rRNAs.

DISCUSSION

In this study, we focused on the early events following *M. tuberculosis* infection in the nonhuman primate model of tuberculosis. The most striking findings of this study were that the first granulomas observed in the lungs were already caseous and that this occurred by 4 weeks postinfection. In monkeys with active TB, a range of granuloma types can be seen, including solid (i.e., those structures comprised primarily of dense aggregates of viable appearing epithelioid macrophages), neutrophilic (i.e., foci with extensive granulocytic infiltrates and/or central areas of suppuration), and caseous granulomas (3). One possible scenario we considered was that lesions progressed from cellular to necrotic to caseous granulomas. However, in the present study, only caseous lesions were observed up to 6 weeks postinfection, supporting an alternative hypothesis that caseation occurs early in granuloma formation, per-

haps shortly after macrophages in the lungs are infected. The local immune responses early after infection were studied, and truly specific T-cell responses were difficult to detect prior to 4 weeks postinfection. In general, responses were observed in the draining lymph nodes prior to in the blood. This suggests a slow induction of T cell responses, which is also observed in the murine model but is distinct from most bacterial and viral infections. However, between 4 and 6 weeks postinfection, the T-cell responses increased and a broader array of *M. tuberculosis* antigens was recognized.

Early after infection, enlargement of hilar lymph nodes was observed, and by 5 weeks postinfection, grossly visible localized granulomas in draining hilar lymph nodes, the nodal component of the classic Ghon complex, could be seen. The presence of microscopic granulomas distal to the initial site of infection (right upper lobe) and on opposite sides of the mediastinum suggests that hematogenous spread likely occurs after infection (4 weeks). This is further evidenced by *M. tuberculosis* growth in two of the axillary lymph nodes, which we have rarely seen in monkeys with latent infection or active disease at later stages of infection. Pulmonary lesions observed in this model are strikingly comparable to human tuberculous lung pathology not only in the histopathologic characteristics but also the spectrum of granuloma types observed. Large human cohort studies have demonstrated the presence of pulmonary infiltrates, hilar adenopathy, and TST conversion within 2 months after infection (15). In the mouse model, we and others have documented early immunologic events and granuloma formation (9, 12, 22) seen as early as 2 to 4 weeks postinfection; however, the structure of granulomas in the murine lung is markedly different from that seen in human TB. In the guinea pig, an early stage of cellular granuloma formation, including CD8 and CD4 T cells, occurs at 2 weeks, followed by more developed caseous granuloma formation by 3 weeks postinfection (25). Lastly in the rabbit model, the presence of both caseous and noncaseous granulomas occurs between 2 to 4 weeks after aerosol infection with *Mycobacterium bovis* (used as a model of *M. tuberculosis* infection) (13).

The presence of only caseous granulomas in the lungs at these early time points after infection was novel and surprising. Our previous and ongoing histologic analysis of lesions within monkeys with active disease often reveal several concurrent types of granulomatous lesions within the same monkey (Fig. 2) (3). This led to our hypothesis that granuloma formation progressed as follows: unstructured aggregates of macrophages surrounding a few infected cells, T cells migrating to the site (forming more architecturally organized solid cellular granulomas), followed by necrosis if the bacteria continued to proliferate, and subsequent caseation. In latently infected monkeys, we generally observe caseous or mineralized lesions intermixed with completely fibrotic granulomas (data not shown). We speculate that the presence of extensive caseation in early granulomas reflects a robust and localized response in which a high degree of intracellular killing with resulting necrosis occurs as an early adaptive response to the pathogen. These areas of necrosis and caseation are hypoxic, which also likely limits bacterial growth (unpublished data). As T cells infiltrate the lungs, they are likely to migrate to the infected macrophages, delineating the granuloma. All the granulomas observed in the lungs had a thin rim of lymphocytes surrounding the macrophage and caseous layers of the structure. It may be that solid or cellular granulomas observed in active disease are the result of bacteria infecting macrophages when there is an established T-cell response in the lungs; this may limit the caseation observed. Caseation may then be the result of a combination of host and bacterial factors and may reflect the intimate and long-term relationship between mycobacteria and the human host involved ultimately in disease outcome. Further studies into the factors contributing to granuloma formation in this model may resolve these questions.

T-cell responses in the blood, airways, hilar lymph nodes, and lungs were compared. In general, antigen-specific responses were observed in the draining lymph nodes prior to the blood. Most of the monkeys who responded to *M. tuberculosis* antigens by PBMC ELISPOT also had responses in the BAL fluid and hilar lymph node responses. In most cases, IFN-γ responses from BAL cells correlated to responses in PBMCs. In contrast, responses in the hilar lymph node were broader and stronger than in PBMC, reflecting the localized nature of *M. tuberculosis* infection. Of note, all hilar lymph nodes in monkeys infected for 4 or more weeks were positive for *M. tuberculosis* CFU and were enlarged following infection. Very few T cells were obtained from the lungs of acutely infected monkeys, since there was only minimal pathology, but enrichment of T cells could be seen in the granulomatous lung tissue (by 5 and 6 weeks). Due to the paucity of T cells in the lung, there were only 2 monkeys in which mycobacterial antigen-specific IFN-γ production from lung T cells could be measured. Both samples had positive responses to at least two antigens.

While there does appear to be a systemic immunologic response early after infection as demonstrated by PBMC ELISPOT, our experience with this model to date has shown that these responses are not necessarily maintained throughout the course of infection (data not shown). This is particularly true among monkeys that develop latent infection (no clinical signs of TB disease despite infection) in which PBMC responses often return to preinfection levels (3). This has important clinical and practical implications, as blood is an easily accessible specimen for diagnostic use in humans, yet it may not reflect the localized immune response. Similar findings have been described in which BAL fluid and PBMC IFN-γ and TNF responses to purified protein derivative were compared among *M. tuberculosis*-infected persons and healthy controls. Positive responses in the BAL fluid but not in PBMCs were demonstrated among patients with *M. tuberculosis* infection compared to controls (2).

This study provided an opportunity to compare the "compartmentalization" of T-cell phenotypes during early infection. There were clear distinctions in activation phenotypes of the T cells in the blood, airways (from BAL cells), draining lymph nodes, and lungs. Only a subset of T cells in the blood were positive for activation markers, with a larger percentage of CD4 cells than CD8 T cells being activated. In contrast, the majority of T cells obtained by BAL were highly activated. The T cells in the hilar lymph nodes had a variable activation pattern, with the CD8 T cells showing much less activation than CD4 T cells, suggesting that priming of CD8 T cells may occur later in the infection or that activated CD8 T cells have already left the lymph node at these early time points. The

characterization of activation signals observed were dependent on the specific immunologic compartment, with cells in the airways being the most activated. This suggests differential regulation of activation, perhaps by local cytokine environment or antigen-presenting cells in each compartment. It may be important to downregulate the immune response within the granulomas to limit inflammation. Even though the BAL cells were the most activated, the BAL fluid did not generally contain culturable bacteria in these early infection monkeys, so the antigen load at the site was unlikely to be driving the activation phenotype. The presence of CD29 expression among lung and BAL cells and not PBMCs suggests that CD29 plays a role in lymphocyte migration to the site of infection, as CD29 can function as a receptor for adhesion molecules. Similar differences in CD29 and CD69 expression among human lung sections and PBMCs has been described previously (16).

Similarly, greater chemokine receptor expression was observed in the airways compared to the PBMC and lymph node compartments. Of note, CCR5 single positive cells were rarely seen in any compartment, suggesting that $CXCR3^+$ cells can gain expression of CCR5 in certain environments, or that double positive cells are drawn to certain sites. This pattern has also been observed in human T cells in which the expression of CXCR3 and CCR5 are much greater than the PBMCs (16). It does appear that in the later weeks of infection, there is an increase in double positive ($CXCR3^+$ $CCR5^+$) cells in the lungs, especially in the CD4 T-cell subset, suggesting evolution of the response as the granulomas develop. The expression of CXCR3 chemokines in the early granulomas is very strong, and we have shown previously that expression of CCL5 is present as well (although at a lower level) (7). Thus, these chemokines may be important in drawing cells to the granuloma. However, the extremely high expression of CXCL9 at the infection site may also act to modulate T-cell effector function in the granuloma or actually prevent cells from trafficking to the site. It is well established that high concentrations of chemokines can stop cells from migrating toward the signal.

There are limitations to the current study, the primary one being the sample size. Nonetheless, these eight monkeys provide a snapshot of the early events following infection, and this has not been previously studied either in humans or in a model so close to human TB. Given the cost and resource limitations of macaques, only limited data are available from uninfected monkeys for comparison. Functional immunologic assays from the lung were limited by the paucity of T cells found. On occasion, microscopic granulomas were found without being observed on gross examination (for example, at 4 weeks postinfection). Such sampling error could have minimized the degree of pathology observed given the localized nature of the infection. Like human studies, the genetic diversity of monkeys results in an inherent degree of animal-to-animal variability and, therefore, heterogeneity of data is seen. Previous infection with bacterial or parasitic pathogens could potentially cause nonspecific pulmonary immune stimulation that could alter the immune response. Lastly, it is important to recognize that development of the cynomolgus monkey TB model is ongoing.

As shown in the current study, the primate model can be used to assess the bacterial burden and immunologic events that occur within the lung and mediastinal lymph nodes over time. While expensive and limited in resource, unlike other animal models of *M. tuberculosis* infection, immunologic reagents are readily available for use. Moreover, this is currently the only animal model of *M. tuberculosis* infection in which a true state of latent infection exists, thus allowing an opportunity to understand important events in establishing latent infection and, in turn, the critical events that predict reactivation of TB. Given the phylogenetic similarities between human and nonhuman primates, as well as the comparable findings at the level of granulomatous lesions and disease outcomes, the results of studies in this model should be very relevant to human *M. tuberculosis* infections. This model holds distinct promise in our understanding of the host-pathogen interaction in TB.

ACKNOWLEDGMENTS

This research was supported by NIH RO1 HL68526 and HL075845 (J.L.F.), Ellison Medical Foundation (J.L.F.), Infectious Disease Society of America Harold Bayer/Neu Fellowship Award (P.L.L.), NIH T32 AI49820 (P.L.L.), and NIH K08 AI63101 (P.L.L.).

We are grateful to Corixa, Inc., and to the NIH Tuberculosis Reagent Contract (NIH NIAID NO1-AI-40091, John Belisle, principal investigator) for supplying the *M. tuberculosis* antigens for immunologic assays. We acknowledge the contributions of Craig Fuller, who performed the initial in situ hybridization of monkey samples, and members of the Flynn lab for helpful discussion. We also thank the staff at the Division of Laboratory Animal Research for animal husbandry.

REFERENCES

1. **Algood, H. M., P. L. Lin, D. Yankura, A. Jones, J. Chan, and J. L. Flynn.** 2004. TNF influences chemokine expression of macrophages in vitro and that of CD11b+ cells in vivo during Mycobacterium tuberculosis infection. J. Immunol. **172:**6846–6857.
2. **Barry, S. M., M. C. Lipman, B. Bannister, M. A. Johnson, and G. Janossy.** 2003. Purified protein derivative-activated type 1 cytokine-producing CD4+ T lymphocytes in the lung: a characteristic feature of active pulmonary and nonpulmonary tuberculosis. J. Infect. Dis. **187:**243–250.
3. **Capuano, S. V. I., D. A. Croix, S. Pawar, A. Zinovik, A. Myers, P. L. Lin, S. Bissel, C. Fuhrman, E. Klein, and J. L. Flynn.** 2003. Experimental *Mycobacterium tuberculosis* infection of cynomolgus macaques closely resembles the various manifestations of human *M. tuberculosis* infection. Infect. Immun. **71:**5831–5844.
4. **Choi, Y. K., B. A. Fallert, M. A. Murphey-Corb, and T. A. Reinhart.** 2003. Simian immunodeficiency virus dramatically alters expression of homeostatic chemokines and dendritic cell markers during infection in vivo. Blood **101:** 1684–1691.
5. **Fallert, B. A., and T. A. Reinhart.** 2002. Improved detection of simian immunodeficiency virus RNA by in situ hybridization in fixed tissue sections: combined effects of temperatures for tissue fixation and probe hybridization. J. Virol. Methods **99:**23–32.
6. **Flynn, J. L., A. Cooper, and W. R. Bishai.** 2005. Animal models of tuberculosis, p. 547–560. *In* S. T. Cole, K. D. Eisenach, D. N. McMurray, and W. R. Jacobs, Jr. (ed.), Tuberculosis and the tubercle bacillus. ASM Press, Washington, D.C.
7. **Fuller, C. L., J. L. Flynn, and T. A. Reinhart.** 2003. In situ study of abundant expression of proinflammatory chemokines and cytokines in pulmonary granulomas that develop in cynomolgus macaques experimentally infected with *Mycobacterium tuberculosis*. Infect. Immun. **71:**7023–7034.
8. **Gormus, B. J., J. L. Blanchard, X. H. Alvarez, and P. J. Didier.** 2004. Evidence for a rhesus monkey model of asymptomatic tuberculosis. J. Med. Primatol. **33:**134–145.
9. **Jung, Y. J., L. Ryan, R. LaCourse, and R. J. North.** 2005. Properties and protective value of the secondary versus primary T helper type 1 response to airborne Mycobacterium tuberculosis infection in mice. J. Exp. Med. **201:** 1915–1924.
10. **Langermans, J. A., T. M. Doherty, R. A. Vervenne, T. van der Laan, K. Lyashchenko, R. Greenwald, E. M. Agger, C. Aagaard, H. Weiler, D. van Soolingen, W. Dalemans, A. W. Thomas, and P. Andersen.** 2005. Protection of macaques against Mycobacterium tuberculosis infection by a subunit vaccine based on a fusion protein of antigen 85B and ESAT-6. Vaccine **23:**2740–2750.
11. **Langermans, J. A. M., P. Andersen, D. van Soolingen, R. A. W. Vervenne, P. A. Frost, T. van der Laan, L. A. H. van Pinsteren, J. van den Hombergh, S. Kroom, I. Peekel, S. Florquin, and A. W. Thomas.** 2001. Divergent effect

of bacillus Calmette-Guerin (BCG) vaccination on Mycobacterium tuberculosis infection in highly related macaque species: implications for primate models in tuberculosis vaccine research. Proc. Natl. Acad. Sci. USA **98:** 11497–11502.

12. **Lazarevic, V., A. J. Myers, C. A. Scanga, and J. L. Flynn.** 2003. CD40, but not CD40L, is required for the optimal priming of T cells and control of aerosol M. tuberculosis infection. Immunity **19:**823–835.
13. **Lurie, M. B.** 1932. The correlation between the histological changes and the fate of living tubercule bacilli in the organs of tuberculous rabbits. J. Exp. Med. **55:**31.
14. **McMurray, D. N., F. M. Collins, A. M. Dannenberg, Jr., and D. W. Smith.** 1996. Pathogenesis of experimental tuberculosis in animal models. Curr. Top. Microbiol. Immunol. **215:**157–179.
15. **Poulsen, A.** 1951. Some clinical features of tuberculosis. Acta Tuberc. Scand. **33:**37–92.
16. **Raju, B., C. F. Tung, D. Cheng, N. Yousefzadeh, R. Condos, W. N. Rom, and D. B. Tse.** 2001. In situ activation of helper T cells in the lung. Infect. Immun. **69:**4790–4798.
17. **Reinhart, T. A., B. A. Fallert, M. E. Pfeifer, S. Sanghavi, S. Capuano III, P. Rajakumar, M. Murphey-Corb, R. Day, C. L. Fuller, and T. M. Schaefer.** 2002. Increased expression of the inflammatory chemokine CXC chemokine ligand 9/monokine induced by interferon-gamma in lymphoid tissues of rhesus macaques during simian immunodeficiency virus infection and acquired immunodeficiency syndrome. Blood **99:**3119–3128.
18. **Rhoades, E. R., A. M. Cooper, and I. M. Orme.** 1995. Chemokine response in mice infected with *Mycobacterium tuberculosis*. Infect. Immun. **63:**3871–3877.
19. **Richter, C. B., N. D. M. Lehner, and R. V. Hendrickson.** 1984. Primates, p. 305. *In* J. G. Fox, B. J. Cohen, F. M. Loew (ed.), Laboratory animal medicine. Academic Press, Inc., San Diego, Calif.
20. **Sadek, M. I., E. Sada, Z. Toossi, S. K. Schwander, and E. A. Rich.** 1998. Chemokines induced by infection of mononuclear phagocytes with mycobacteria and present in lung alveoli during active pulmonary tuberculosis. Am. J. Respir. Cell Mol. Biol. **19:**513–521.
21. **Saukkonen, J. J., B. Bazydlo, M. Thomas, R. M. Strieter, J. Keane, and H. Kornfeld.** 2002. β-Chemokines are induced by *Mycobacterium tuberculosis* and inhibit its growth. Infect. Immun. **70:**1684–1693.
22. **Serbina, N. V., V. Lazarevic, and J. L. Flynn.** 2001. CD4+ T cells are required for the development of cytotoxic CD8+ T cells during *Mycobacterium tuberculosis* infection. J. Immunol. **167:**6991–7000.
23. **Tribe, G. W., and A. E. Welburn.** 1976. Value of combining the erythrocyte sedimentation rate test with tuberculin testing in the control of tuberculosis in baboons. Lab. Anim. **10:**39–46.
24. **Tsai, M. C., S. Chakravarty, G. Zhu, J. Xu, K. Tanaka, C. Koch, J. Tufariello, J. Flynn, and J. Chan.** 2006. Characterization of the tuberculous granuloma in murine and human lungs: cellular composition and relative tissue oxygen tension. Cell. Microbiol. **8:**218–232.
25. **Turner, O. C., R. J. Basaraba, and I. M. Orme.** 2003. Immunopathogenesis of pulmonary granulomas in the guinea pig after infection with *Mycobacterium tuberculosis*. Infect. Immun. **71:**864–871.
26. **Walsh, G. P., E. V. Tan, E. C. de la Cruz, R. M. Abalos, L. G. Villhermonsa, L. J. Young, R. V. Cellona, J. B. Nazareno, and M. A. Horwitz.** 1996. The Philippine cynomolgus monkey (Macaca fascularis) provides a new nonhuman primate model of tuberculosis that resembles human disease. Nat. Med. **2:**430–436.
27. **World Health Organization.** March 2006, last date modified. Tuberculosis. [Online.] http://www.who.int/mediacentre/factsheets/fs104/en/index.html.

Editor: V. J. DiRita